Jordanian Journal of Engineering and Chemical Industries

Print ISSN: 2616 - 9584 Online ISSN: 2617 - 720X

Thermodynamic and Adsorption Studies of Salvia Officinalis as A Green Corrosion Inhibitor for Steel at 1 M Sulfuric Acid

Shatha N. Badarneh*[1], Salah H. Aljbour[2], Toqa T. Al-Btoush[1] and Mohammad A. Al-Awamleh[1]

[1]Department of Chemical Engineering, Al-Karak University College, Al-Balqa Applied University, Salt 19117, Jordan
[2]Department of Chemical Engineering, College of Engineering, Mutah University, Karak, 61710, Jordan

Abstract

This study includes the temperature effect on the performance of the corrosion inhibitor (Salvia officinalis) that is used in different concentrations (570, 1119, 1647) ppm in acidic medium (1M H_2SO_4) of mild steel using the weight loss method. The result has shown that the extract is a good inhibitor of the corrosion of mild steel in H_2SO_4. The corrosion rate drops with an increase in the concentration of inhibitors and rises with an increase in temperature. In contrast, the inhibition efficiency grows with an increase in the inhibitor concentration and reduces with an increase in temperature. Standard free energy of adsorption estimated based on the Langmuir model was -26.66 kJ/mol at 22 °C. The adsorption of this inhibitor on the mild steel surface conforms to Langmuir adsorption isotherm.

Paper type: Research Paper
Keywords: Salvia Officinalis, Corrosion Inhibitor, Mild Steel, Sulfric Acid, Thermodynamic Properties.

Citation: Badarneh, S. N., S. H. Aljbour, T. T. Al-Btoush, and M. A. Al-Awamleh, "Thermodynamic and Adsorption Studies of Salvia Officinalis as a Green Corrosion Inhibitor for Steel at 1 M Sulfuric Acid," *Jordanian Journal of Engineering and Chemical Industries*, Vol. **9**, No. 1, pp: 25–43 (2026).

1. Introduction

Mild steel (MS) is used widely in infrastructure consequent its approved mechanistic features, malleability, strength, availability, and low price. It finds large use across industries. For example, in pipelines, reactors, storage tanks, separation units, gas cylinders, and heat exchangers Acidic solutions are extensively utilized in considerable industrial processes, involving steel pickling, industrial acid cleaning, descaling, and oil-well acidizing (Ibrahim et al., 2022). The most generally used acids are hydrochloric acid (HCL), sulfuric acid (H_2SO_4), and nitric acid (HNO_3) (Al-Rashed et al., 2022). Corrosion of mild steel in these environments presents a complicated defiance. Corrosion characteristics of steel in harsh mineral acid media have been widely investigated (Javidi et al., 2024; Ou et al., 2025; Panossian et al., 2012). Organic and inorganic inhibitors are the best way to protect steel from corrosion, specifically in acidic environments (Ahmed et al., 2024; Mamedov et al., 2019).

Inorganic corrosion inhibitors are extensively used since they remain effective over wider temperature ranges and can provide protective performance for long durations (Ahmed et al., 2024) In contrast, organic inhibitors are cheap, eco-friendly, and safer (Deyab et al., 2023). Because of the above reasons, researchers have worked hard to identify the effective organic compounds in many herbs that work as corrosion inhibitors (Eddy et al., 2022). Organic compounds act to inhibit corrosion by virtue of their heteroatom (N,S,O) content, electronegativity of functional groups and by promoting adsorption through the presence of conjugated double bonds. The organic compound forms covalent bonds with the metal surface to create an impermeable film which protects the metal from attack. The film alters the electrical double layer present at the metal interface; this barrier is located in close proximity to the metal surface

* Corresponding author: E-mail: shathabadarneh@bau.edu.jo ORCID: **0009-0002-4130-1312**
Received: 26/November/2025 Revised: 23/Feburary/2026

Jordanian Journal of Engineering and Chemical Industries (JJECI), Vol.9, No.1, 2026, pp: 25-43 Accepted: 04/March/2026

and has two functions: it prevents the access of corrosive species to the metal surface by blocking the active sites and reduces the diffusion of corrosive species to the metal surface by slowing down the reaction between the corrosive species and the metal surface (de Souza Morais et al., 2023). Many Studies investigated various organic compounds as green inhibitors of steel (Lavanya et al., 2024; Mo et al., 2016; Singh et al., 2016).

Salvia officinalis is an aromatic herb related to the mint family. Salvia officinalis is a well-known herb used as a traditional medicine for the treatment of most types of ailments. In addition, people used it as a type of flavoring to prepare different types of foods. Salvia officinalis has enormous numbers of diterpenoids and phenolic acids involving novel caffeic acid, polyphenols, phenolic glycosides, flavonoids, and metabolites such as superionic acid, sage coumarin, etc (Babiker, 2024). Many researchers studied Saliva officinalis as a green corrosion inhibitor. For example, (Rodríguez-Torres et al., 2015) evaluated the effect of Salvia officinalis extract as a carbon steel corrosion inhibitor (1018) in 0.5M H2SO4 by comparing gravimetric and electrochemical data. A combination of three temperatures (25°C, 40°C and 60°C) and three different Salvia extract concentrations (100ppm, 200ppm, 300ppm) were used. The results showed that the Salvia extract is a very efficient corrosion inhibitor for the first 12 hours of immersion, however, after this immersion period, the Salvia extract started to desorb from the metal surface and therefore significantly reduced the inhibitor's protection efficiency. Babiker and M. E.,2024 evaluated the corrosion inhibitory effects of Salvia officinalis extract on Zinc in 0.5M H2SO4 employing gravimetric data (weight loss method) and chemical analysis. The experiments were performed over temperature ranges of 20-45°C, with Salvia concentrations up to 600ppm. Even though the inhibition performance of Salvia was clearly shown through the experimental results, no information on the immersion time was provided.

Although there are many studies on plant-based green corrosion inhibitors (e.g., Salvia officinalis), these have generally been limited to short-term testing with low inhibitor levels or have focused only on either the adsorption and/or thermodynamics of the inhibitor. Therefore, there is an obvious need for a study that investigates the long term protective properties of Salvia officinalis when used as a corrosion inhibitor for mild steel in highly corrosive media (i.e., concentrated 1.0 M H_2SO_4) under conditions that include extended immersion times, higher inhibitor levels than those typically tested, and complete kinetic, thermodynamic, and adsorption isotherm analyses. This will be necessary in order to evaluate both the potential for long term use of Salvia officinalis as a corrosion inhibitor for mild steel in such environments and its practical applications as a green inhibitor under conditions found in industrial use.

The present study demonstrates the varying temperature effect (22, 35, 45) °C on the behavior of Saliva *officinalis* as a green corrosion inhibitor, with the concentrations being: 570, 1119, 1647 ppm in 1M H_2SO_4 during a long time 48 hours. In addition, activity energy, thermodynamic properties, and various isotherm models are studied.

2. Materials and Methods

2.1 Materials

2.1.1 Mild steel nails

Mild steel nails with 30 mm length and 5 mm diameter , they were rinsed with distilled water, and dried before use.

2.1.2 Preparation of Acidic Solution

500 ml of 1.0 M H_2SO_4 was used as an acidic media; it was prepared by using Sulfuric acid (98% w/w) and De-ionized water. The solution was prepared according to dilution formula:

$$M1.V1 = M2.V2 \quad (1)$$

Approximately 27.2 ml of concentrated H_2SO_4 was slowly added to 300 ml of distilled water while stirring under a fume hood, then diluted it to a final volume of 500 ml.

2.1.3 Preparation of Inhibitor Essential Oil Extract

Fresh *Salvia officinalis* (common sage) was collected from Irbid, Jordan (**Figure 1**). Leaves and stems of sage were rinsed with deionized water, air-dried, and prepared for use. 20 g of Sage (leaves and stems) were weighed using a calibrated analytical balance and ready to use. Meanwhile a hot water bath was prepared to use; the water bath temperature controller set point was adjusted to 100°C. 100 ml of De-ionized water was heated in a beaker using a hot plate until reaching 100°C (boiling point), then the weighed 20 g of sage (leaves and stems) were immersed in the boiled De-ionized water, covered with glass petri dish to prevent evaporation of extract, and then the beaker was submersed in the (approximately 100°C) hot water bath for 24 hours. After 24 hours, the 100 ml Sage extract was ready. Extract was separated from the leaves and stems by filtration. The pure sage extract was placed in a clean, labeled beaker and stored in a refrigerator at 4°C.

Fig. 1. Salvia officinalis plant.

2.2 Experimental Methods

2.2.1 Mild Steel characterization

Chemical composition of mild steel used in this study was ascertained using a Sci-APS handheld XRF analyzer. The test indicated a composition characteristic of commercial general low-carbon steel grades.

2.2.2 ATR-FTIR Analysis of Sage

ATR-FTIR Spectroscopy was utilized to determine the chemical structure of the functional groups contained within Sage. The samples were powdered and dried in a drying oven at 40° C before being analyzed by ATR-FTIR. Spectra for FTIR were acquired on a Bruker Alpha II with the sample scanned from 4000–400 cm^{-1} at a resolution of 4 cm^{-1}. The resultant FTIR spectra were analyzed to determine which absorption peaks corresponded to the functional groups responsible for the corrosion inhibition.

2.2.3 Nutritional Composition of Sage

Dried powdered Sage sample were analyzed for nutritional composition using a device called FoodScan Lab 78810 food analyzer, following AOAC standard methods (McCleary, 2023).

2.2.4 Minerals Content of Sage

Mineral content of the sage sample was quantified by atomic absorption spectroscopy (Flame Mode) using a PerkinElmer AAnalyst 400. Samples were prepared by appropriate dilution and acid digestion before analysis is conducted.

2.2.5 Vitamins content of Sage

An aqueous extract of sage was prepared to quantify vitamin content in sage Analysis was performed by HPLC (Shimadzu LC-20) with C18 column and UV detection at 280 nm, using methanol: water: acetic acid (70:28:2) as mobile phase at 1 mL/min.

2.2.6 Proximate Composition of Sage

Proximate analysis for sage was conducted according to standard methods described by the Association of Official Analytical Chemists (AOAC) and ASTM standards for biomass characterization to evaluate moisture, ash, volatile matter, and fixed carbon content (McCleary, 2023). 100 g of sage fresh leaves were collected locally from Irbid, Jordan. The leaves were washed with distilled water to remove dust and surface contaminants, then air-dried at room temperature and further oven-dried at 60 °C until a constant weight was achieved. Dried leaves were ground and sieved through a 250 µm mesh. The powdered sample was stored in airtight container at room temperature until analysis. For moisture content calculations, approximately 2 g of the dried powdered sample was weighed into a pre-weighed heat-resistant crucible and placed in a hot drying oven at 105 ± 2 °C for 24 hours. The crucible was then cooled in a desiccator and reweighed. Moisture content was calculated as follows (ASTM International, 2015), (AOAC, 2019):

$$\text{Moisture } (\%) = \left(\frac{W_1 - W_2}{W_1}\right) * 100 \quad (2)$$

W_1: Initial weight of sample
W_2: Weight of sample after drying

For ash content calculations, approximately 2 g of the dried powdered sample was placed in a crucible (pre-weighed) and incinerated for 4 hours in a muffle furnace at 600 ± 25 °C until a white ash was obtained, then the crucible was cooled in a desiccator and weighed. Ash content was calculated as follows (ASTM International, 2013):

$$\text{Ash } (\%) = \left(\frac{W_3}{W_1}\right) * 100 \quad (3)$$

W_3: Weight of ash

For volatile matter calculations, approximately 2 g of the dried powdered sample was placed in a lidded pre-weighed crucible (to limit oxygen exposure) and heated in a muffle furnace at 950 ± 20 °C for 7 minutes. After cooling in a desiccator, the residue was weighed. Volatile matter was calculated as follows (ASTM International, 2020):

$$\text{Volatile Matter } (\%) = \left(\frac{W_1 - W_4}{W_1}\right) * 100 \quad (4)$$

W_4: Weight after volatile matter removal
Fixed carbon was estimated by difference using the following formula:

$$\text{Fixed Carbon } (\%) = 100 - (Moisture + Ash + Volatile\ Matter) \quad (5)$$

2.2.7 Weight Loss Measurements

Mild steel nails were thoroughly rinsed with acetone, dried and weighed using analytical balance before immersion in solutions; all weights were recorded preparing for weight loss calculations. The experimental setup and immersion procedure are illustrated in **Figures 2 and 3**.Three different runs were conducted as follows:

1st run - 10 ml of sage liquid extract (~570 ppm of extract**)- : samples of mild steel nails were immersed in 500 ml of 1.0 M H_2SO_4 (Blank), and other samples were immersed in 500 ml of 1.0 M H_2SO_4 including (10 ml) of sage liquid extract (Blank + Inhibitor) with a total solution of 510 ml, all these samples were examined at 48 hours of immersion time and 22°C. Same procedures were followed for different samples at the same 48 hours of immersion time but at different temperatures (35°C & 45°C respectively). A hot water baths were used to ensure continuous required thermal conditions, with a temperature controller set points of 35°C &45°C.

2nd run - 20 ml of sage liquid extract (~1119 ppm of extract**)-: samples of mild steel nails were immersed in 500 ml of 1.0 M H_2SO_4 (Blank), and other samples were immersed in 500 ml of 1.0 M H_2SO_4 including (20 ml) of sage liquid extract (Blank + Inhibitor) with a total solution of 520 ml, all these samples were examined at 48 hours of immersion time and 22°C. Same procedures were followed for different samples at the same 48 hours of immersion time but at different temperatures (35°C & 45°C respectively). A hot water baths were used to ensure continuous required thermal conditions, with a temperature controller set points of 35°C & 45°C.

3rd run - 30 ml of sage liquid extract (~1647 ppm of extract**)-: samples of mild steel nails were immersed in 500 ml of 1.0 M H_2SO_4 (Blank), and other samples were immersed in 500 ml of 1.0 M H_2SO_4 including (30 ml) of sage liquid extract (Blank + Inhibitor) with a total solution of 530 ml, all these samples were examined at 48 hours of immersion time and 22°C. Same procedures were followed for different samples at the same 48 hours of immersion time but at different temperatures (35°C & 45°C respectively). A hot water baths were used to ensure continuous required thermal conditions, with a temperature controller set points of 35°C & 45°C.

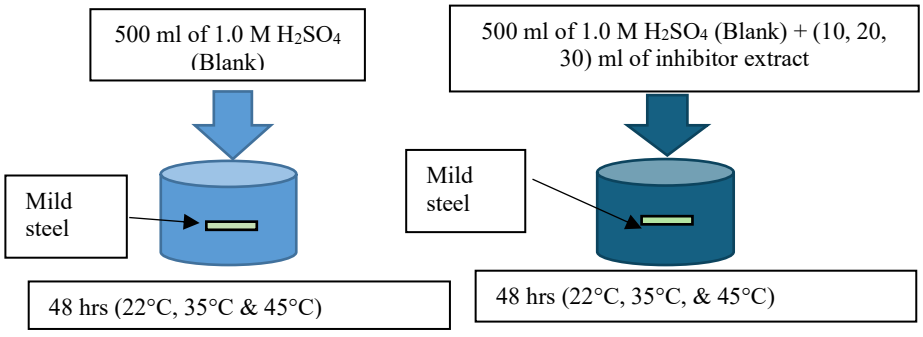

Fig. 2. A schematic diagram showing how mild steel is immersed in 1.0 M H_2SO_4 at 48 hours and at various temperatures with or without an inhibitor extract.

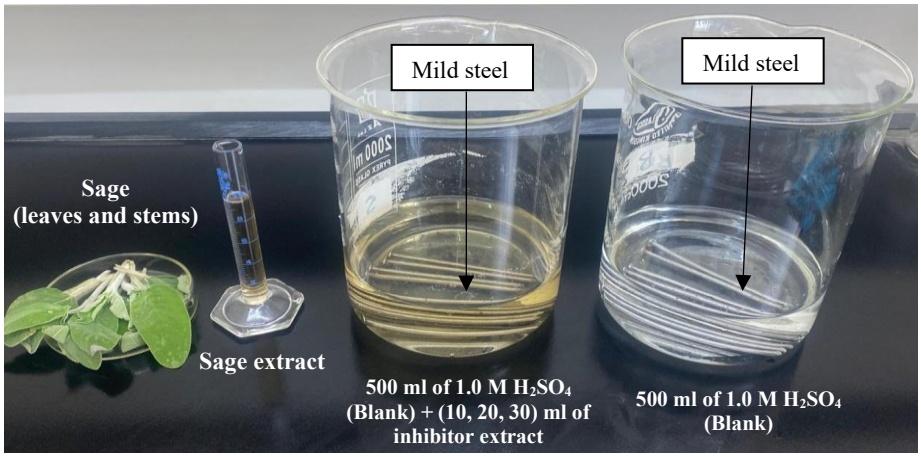

Fig. 3. Experiment setup and materials.

Note: After each immersion period, samples were removed from the solution, washed with acetone, dried, and weighed using analytical balance. All weights were recorded preparing for weight loss calculations.

** As boiled water was used in this study for sage extraction, which is considered less efficient extraction method compared to hydrodistillation method, it is assumed that the extraction yield of the main components of Sage is 15%, this assumption was based on (Vieira, Ferreira, & Neves, 2020(Xu et al., 2021). According to (Velamuri et al., 2020); the molecular weight of major components in Sage (flavonoids) was (270 g/mol). The estimated approximate value of extract concentration (ppm) found in 10 ml inhibitor extract was calculated as follows:

$$\text{Sage dry weight (g)} = Fresh\ sage\ (g) * (1 - moisture\ \%)$$

$$\text{Assumed extracted (g)} = Sage\ dry\ weight\ (g) * 15\ \%$$

$$\text{Concentration of extract in 100 ml hot water (ppm)} = \frac{Assumed\ extracted(mg)}{0.1\ (L)}$$

$$\text{Concentration of extract after dillution with acid (ppm)} = \frac{Concentration\ of\ extract\ in\ 100\ ml\ hot\ water\ (ppm) * Volume\ of\ inhibitor\ extract\ added\ (ml)}{Volume\ of\ inhibitor\ extract\ added\ (ml) + Volume\ of\ acid\ (ml)}$$

a) Weight Loss calculations = Mild steel weight before immersion – Mild steel weight after immersion
b) Inhibition Efficiency calculations (Murthy & Vijayaragavan, 2014):

$$\%\ \text{IE} = 100 * \frac{\Delta W^{\circ} - \Delta W}{\Delta W^{\circ}} \quad (6)$$

% IE: Inhibition Efficiency

ΔW°: Weight loss of mild steel without inhibitor

ΔW: Weight loss of mild steel with inhibitor

c) Degree of Surface Coverage calculations (Murthy & Vijayaragavan, 2014):

$$\theta = \frac{\Delta W^{\circ} - \Delta W}{\Delta W^{\circ}} \quad (7)$$

θ: Degree of Surface Coverage

As illustrated in Equation 6 and 7 , Inhibition Efficiency is proportional to surface area coverage (%IE = 100 × θ). The correlation assumes that the primary effect of inhibitors on corrosion is via adsorption of the inhibitor molecules onto metal surfaces (active sites). However, it should be noted that this model does not account for the potential effects of the inhibitor on kinetic reactions, formation of multilayer adsorption films, etc. The percentage of surface area covered by inhibitor molecules can therefore be used as an indicator of "effective" inhibition, but not as an indication of the actual percent of surface area that is physically blocked.

d) Corrosion Rate calculations (Murthy & Vijayaragavan, 2014):

$$\mathrm{CR} = \frac{\Delta W}{Mild\ steel\ surface\ area * Immersion\ time} \quad \text{(for inhibitor sample)} \tag{8}$$

CR: Corrosion rate

For the blank solution $\Delta W = \Delta W^{\circ}$(weight loss without inhibitor). The exposed surface area (A) for the mild steel test samples was estimated based on their original geometric properties. The nails were cylindrical, measuring 3.00 cm in length, 0.50 cm in diameter (radius = 0.25 cm) and the total exposed surface area was found by applying the cylindrical formula:

$$A = 2\pi rL + \pi r^2 \tag{9}$$

The calculated initial surface area of each sample was about 4.91 cm². Since corrosion will likely reduce the surface area during immersion and therefore reduce the amount of mass lost through the weight loss method, we used the original geometric surface area as an approximate standard in this method.

2.3 Thermodynamic and Kinetic Analysis

To understand temperature effects on corrosion and inhibition, activation energy, entropy of activation, and enthalpy of activation parameters to be calculated according the following

Arrhenius Equation -for Activation Energy- (Babiker, 2024):

$$\ln(CR) = \ln A - \frac{E_a}{RT} \tag{10}$$

A plot of ln *(CR)* vs *1/T* will give a line that we can use to calculate the slope and the intercept.

$$\mathrm{Slope} = -\frac{E_a}{R} \tag{11}$$

$$\mathrm{Intercept} = \ln A \tag{12}$$

We can calculate (E_a) and (A) from equations shown above depending on the slope and intercept values concluded from the plot of ln *(CR)* vs *1/T*.

A: Frequency factor ($g \cdot cm^{-2} \cdot h^{-1}$)

E_a: Activation energy (J/mol)

R: Gas constant (8.314 J/mol·K)

T: Absolute temperature (K)

Transition State Equation -for entropy of activation and enthalpy of activation- (Babiker, 2024):

$$\ln\frac{CR}{T} = \ln\frac{R}{N_h} + \frac{\Delta S}{R} - \frac{\Delta H}{RT} \tag{13}$$

A plot of ln *(CR/T)* vs *1/T* will give a line that we can use to calculate the slope and the intercept.

$$\mathrm{Slope} = -\frac{\Delta H}{R} \tag{14}$$

$$\text{Intercept} = \ln\frac{R}{N_h} + \frac{\Delta S}{R} \quad (15)$$

We can calculate (ΔH) and (ΔS) from equations shown above depending on the slope and intercept values concluded from the plot of ln *(CR/T)* vs *1/T*.

Δ*H*: Enthalpy of activation (J/mol)

Δ*S:* Entropy of activation (J/mol·K)

N: Avogadro's number (6.022×10^{23} mol^{-1})

h: Planck's constant (6.626×10^{-34} J·s)

2.3.1 Adsorption Isotherm Models

To study the adsorption process of sage extracts on a mild steel surface, a number of adsorption isotherms have been fitted to the inhibition data obtained from weight loss determinations. The calculated surface coverages (θ) for the various inhibitor concentrations have been utilized in order to determine which isotherm model(s) are applicable for describing the adsorption mechanism.

The following isotherms were considered:

1. Langmuir Adsorption Isotherm

The Langmuir isotherm follows monolayer adsorption. Following Equation is applied (Murthy & Vijayaragavan, 2014):

$$\frac{C}{\theta} = \frac{1}{K_{ads}} + C \quad (16)$$

A plot of C/θ vs *C* will give a straight line if Langmuir isotherm is followed, that we can use to calculate the slope and the intercept.

$$\text{Slope} = 1$$

$$\text{Intercept} = \frac{1}{K_{ads}} \quad (17)$$

We can calculate (K_{ads}) from equations shown above depending on the intercept value concluded from the plot of C/θ vs *C*.
We can use (K_{ads}) value to calculate standard free energy according to the following equation (Murthy & Vijayaragavan, 2014):

$$\text{K}_{\text{ads}} = \left(\frac{1}{55}\right)\left[\exp\left(-\frac{\Delta G^{\circ}_{ads}}{RT}\right)\right] \quad (18)$$

C: Concentration of green inhibitor (mg/L or ppm)
K_{ads}*:* Langmuir adsorption equilibrium constant (L/mg or L/mol)
ΔG°_{ads}*:* Standard free energy of adsorption

55.5: Concentration of water in mol/L (assuming aqueous phase)

Change in Enthalpy (ΔH^{o}) and change in Entropy (ΔS^{o}) can be found using the following equation (Girish, 2025):

$$\ln K_{ads} = -\frac{\Delta H^{o}}{R} * \frac{1}{T} + \frac{\Delta S^{o}}{R} \quad (19)$$

A plot of $\ln K_{ads}$ vs $\frac{1}{T}$ will give a straight line, that we can use to calculate the slope and the intercept.

$$\text{Slope} = -\frac{\Delta H^{o}}{\text{R}} \quad (20)$$

$$\text{Intercept} = \frac{\Delta S^{o}}{\text{R}} \quad (21)$$

We can calculate change in Enthalpy (ΔH^{o}) and change in Entropy (ΔS^{o}) from equations shown above depending on the intercept and slope values concluded from the plot of $ln\ K_{ads}$ vs $\frac{1}{T}$.

2. Freundlich Adsorption Isotherm

The Freundlich isotherm model is used for multilayer adsorption. Following Equation is applied (Freundlich, 1906):

$$\log\theta = \log K_f + \frac{1}{n}\log C \quad (22)$$

A plot of $\log\theta$ *vs* log *C* will give a straight line if Freundlich isotherm is followed, that we can use to calculate the slope and the intercept.

$$\text{Slope} = \frac{1}{n}$$

$$\text{Intercept} = \log K_f$$

We can calculate (K_f) and (n) from equations shown above depending on the slope and intercept values concluded from the plot of $log\,\theta$ *vs log C*. Standard free energy is not calculated for Freundlich isotherm because the equation is imperial.

K_f: Freundlich adsorption capacity constant (L/mg or L/mol)
n: Adsorption intensity

3. Florry-Huggins Adsorption Isotherm

The Flory–Huggins isotherm model consider the size of the adsorbing specimen, assuming non-ideal adsorption on a solid surface. Following Equation is applied (Nikitas, 1984):

$$\log\left(\frac{\theta}{C}\right) = \log K_{fh} + x\log(1-\theta) \quad (23)$$

A plot of $\log(\frac{\theta}{C})$ vs $\log(1-\theta)$ will give a straight line if Florry-Huggins isotherm is followed, that we can use to calculate the slope and the intercept.

$$\text{Slope} = x$$

$$\text{Intercept} = log K_{fh}$$

We can calculate (K_{fh}) and (x) from equations shown above depending on the slope and intercept values concluded from the plot of $\log(\frac{\theta}{C})$ vs $\log(1-\theta)$.
We can use (K_{fh}) value to calculate standard free energy according to the following equation (Murthy & Vijayaragavan, 2014):

$$K_{fh} = \left(\frac{1}{55}\right)\left[\exp\left(-\frac{\Delta G^{\circ}_{ads}}{RT}\right)\right] \quad (24)$$

K_{fh}: Flory–Huggins adsorption equilibrium constant (L/mol)
x: Number of surface sites occupied per inhibitor molecule

Change in Enthalpy (ΔH^o) and change in Entropy (ΔS^o) can be found using the following equation (Girish, 2025):

$$\ln K_{fh} = -\frac{\Delta H^o}{R} * \frac{1}{T} + \frac{\Delta S^o}{R} \quad (25)$$

A plot of $\ln K_{fh}$ vs $\frac{1}{T}$ will give a straight line, that we can use to calculate the slope and the intercept.

$$\text{Slope} = -\frac{\Delta H^o}{\text{R}}$$

$$\text{Intercept} = \frac{\Delta S^o}{\text{R}}$$

We can calculate (ΔH^o) and (ΔS^o) from equations shown above depending on the intercept and slope values concluded from the plot of ln K_{fh} vs $\frac{1}{T}$.

3. Results and Discussion

3.1 Mild Steel Characterization

Chemical composition analysis was determined for mild steel nails using a Sci-APS device -portable XRF analytical instrument- (**Table 1**)

Table 1. Chemical composition of mild steel (Mass %) (Al-Btoush et al., 2026).

Chemical Elements	**Fe**	**Mn**	**Si**	**S**	**Cu**	**Ni**	**C**
Mass %	99.13	0.489	0.163	0.1	0.063	0.034	0.025

The XRF analysis revealed the mild steel sample with predominance of iron (99.13%) with trace amounts of manganese, silicon, sulfur, copper, nickel, and carbon, which is consistent with the typical composition of low-carbon steels (Wang et al., 2022). The extremely low content of 0.025% carbon further verifies the material as mild steel with good ductility but without any corrosion resistance. Low content of alloying constituents such as Ni and Cu produces minimal protective action, making the steel very prone to acid-induced corrosion. The selected mild steel is therefore a good substrate for evaluating the inhibitory performance of sage extract because improvements in corrosion resistance are mostly attributed to the inhibitor rather than intrinsic alloying action.

3.2 Sage characterization

3.2.1 Nutritional Composition of Sage

The proximate composition of sage powder is presented in **Table 2**. Total fat content of the sample is 12.3%, carbohydrates is 42%, and dietary fiber is 41%. Functional groups of these macronutrients interact with metals surfaces to enhance corrosion inhibitory potential by creating a protective barrier against corrosion on metal surface. For example, the hydroxyl, carboxyl and carbonyl groups of carbohydrates (dietary fiber), dietary fat and other dietary components can adsorb onto the metal surface which will reduce contact between the metal surface and the corrosive medium thereby slow down the rate of corrosion. This mechanism is widely reported as one of the primary mechanisms in natural extract-based corrosion inhibitors (Talha, 2025).

Table 2. Nutritional Composition of sage Powder (Al-Btoush et al., 2026).

Composition	**g/100g**
Total Fat	12.3
Saturated Fat	0
Trans Fat	0
Polyunsaturated Fat	0
Monounsaturated Fat	0
Cholesterol	0
Sodium	0
Carbohydrate	42
Dietary Fat	41
Sugar	0
Protein	0
Other Componatns (Minerals and Vitamins)	4.7

3.2.2 Minerals Content of Sage

The mineral composition of sage is listed in **Table 3**. Calcium (1200 mg/100g), potassium (630 mg/100g), and magnesium (305 mg/100g) were present in considerable amounts, while iron (22 mg/100g), zinc (4.2 mg/100g), and manganese (1.5 mg/100g) were present in trace amounts. These minerals affect the adsorption properties of the inhibitor on the metal surface and can cause the formation of protective complexes.

Table 3. Minerals Content of sage (Al-Btoush et al., 2026).

Composition	mg/100g
Calcium	1200
Potassium	630
Magnesium	305
Iron	22
Zinc	4.2
Manganese	1.5

3.2.3 Vitamins content of Sage

High-performance liquid chromatography (HPLC) analysis established various vitamins in sage like vitamin A (0.9 mg/100g), vitamin C (21 mg/100g), vitamin E (9 mg/100g), thiamin (0.07 mg/100g), niacin (6 mg/100g), folate (0.13 mg/100g), and vitamin B6 (1.2 mg/100g). These bioactive compounds possess antioxidant activity and can adsorb on the surfaces of mild steel to shield them against acid-induced corrosion.

Table 4. Minerals Content of sage (Al-Btoush et al., 2026).

Composition	mg/100g
Vitamin A	0.9
Vitamin C	21
Vitamin E	9
Thiamin	0.07
Niacin	6
Folate	0.13
Vitamin B6	1.2

3.2.4 Proximate Composition of Sage

The proximate composition of sage, as reported in **Table 5**, shows that the sample has very low ash (2.9%) and moisture (3.1%), and low fixed carbon (5.0%) with high volatile matter (92.1%). The 3.1% water content present is considerably less than the standard 10–14% advisable for dried plant material (El Euch et al., 2019), ensuring the chemical integrity of bioactive compounds and avoiding deterioration during storage. The extremely high volatile matter content suggests a concentrated concentration of organic components like essential oils, flavonoids, terpenes, and phenolic acids, all of which are proven to be corrosion inhibition sources (Sellami et al., 2012). These compounds contain functional groups like –OH, –OCH_3, and –COOH, which can adsorb onto mild steel surfaces and create an inert film, effectively shielding corrosion sites.

Table 5. Proximate composition of sage (Al-Btoush et al., 2026).

	Moisture	Volatile Matter	Fixed Carbon	Ash
wt%	3.1	92.1	5.0	2.9

3.2.5 ATR-FTIR Analysis of Sage

The FTIR-ATR spectrum for Sage extract in **Figure 4** confirms that there are several functional groups associated with adsorption on the metal surface and with the development of protective films. The wide band at 3250–3350 cm−1 indicates OH stretching of the alcohol and phenol functional group, which may engage in hydrogen bonding and thus surface adsorption. The peaks from 2850 to 2925 cm−1 represent the CH stretching of the aliphatic CH2 and CH3 groups typical of terpene and essential oil components and contribute to the formation of a hydrophobic layer. The bands located at 1700–1730 cm−1 indicate the C=O stretching of esters, aldehydes and carboxyl acid carbonyl groups, which may also be able to interact with the Fe2+/Fe3+ ions to enhance chemisorption. Finally, the band at 1600–1620 cm−1 indicates the C=C stretching of the aromatic ring and represents the presence of the polyphenolic compound class known as flavonoids, which have been shown to have high adsorption efficiencies.

The bands present in 1100–1030 cm^{-1} correspond to C–O stretching vibrations of alcohols, ethers, and phenolic esters, which facilitate adsorption mechanisms. Bands below 900 cm^{-1} are also associated with out-of-plane bending vibrations of aromatic groups. Previous

studies have reported the same functional groups in natural plant inhibitors, testifying to their effectiveness in surface interaction and protective layer formation (Bajrami et al., 2023; Christaki et al., 2023). Hydroxyl, carbonyl, aliphatic, and aromatic groups of sage are adsorption centers, reducing the steel surface-acid medium interaction and hence corrosion resistance.

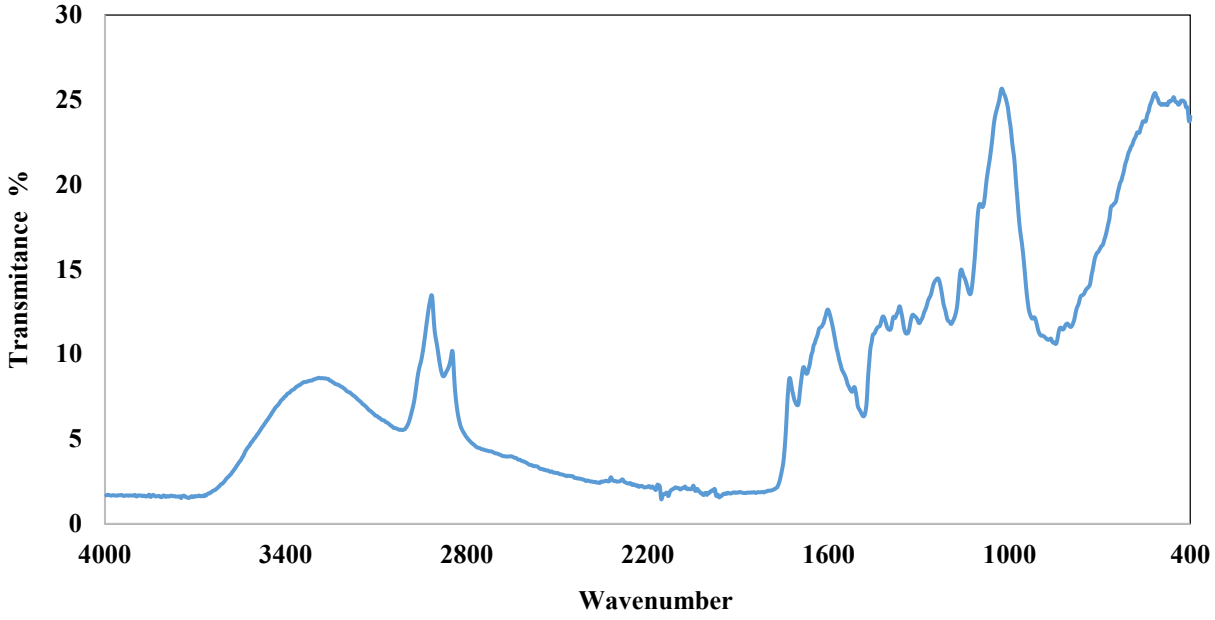

Fig.4 FTIR spectra of sage.

3.3 Effect of Temperature

Temperature is an important variable to consider when evaluating the effects of corrosive environments on corrosion rates. As temperature is increased, the general increase in corrosion rates can be primarily related to a decrease in the overpotential required for hydrogen gas to evolve from the metal surface (Parangusan et al., 2021) . In this study, the impact of temperature on the corrosion inhibition efficiency of mild steel immersed in 1M sulfuric acid containing various concentrations of sage extract was evaluated by measuring mass loss at each of three temperatures (22-45°C) using mass loss measurements. The data shown in **Figure 5** demonstrates that higher concentrations of sage extract resulted in higher values of IE% across all test temperatures. This was found to be a result of increased adsorption and subsequent greater coverage of the metal surface as the concentration of the inhibitor increased.

The level of protection offered by an inhibitor is shown through the inhibitors' overall corrosion inhibition efficiency; this has dramatically increased from 72.16 % to 92.25 % as the concentration of sage extract has risen from 570 ppm to 1647 ppm. The experimental results have also provided evidence for a physical adsorption mechanism; as indicated by the greater inhibition efficiencies observed at ambient temperature (22 °C) compared to elevated temperatures. The decrease in inhibition efficiency of the metal as well as the rise in the corrosion rates of the metal with increasing temperature are consistent with the physical adsorption mechanism described above and would indicate that thermal energy will disrupt or reduce the adsorption of inhibitor molecules. This behavior helps explain that the inhibitor molecules are physically adsorbed onto the metal surface, consistent with the process of physical adsorption (Almahdy et al., 2023). Although some inhibition persists at higher temperatures, the efficiency is much higher at lower temperatures, attributed to the stronger adsorption of inhibitor molecules under such conditions, where the corrosion rate is very low (Ituen et al., 2017). The maximum inhibition efficiency of sage was found to be 92.25% with concentrations of 1647 ppm at 22°C. Similar results were reported by (Babiker, 2024) who achieved a maximum inhibition performance of 92.4% for zinc in 0.5 M Sulfuric Acid at a concentration of 600 ppm and a temperature of 301 K by using sage extract, based on weight loss measurements.

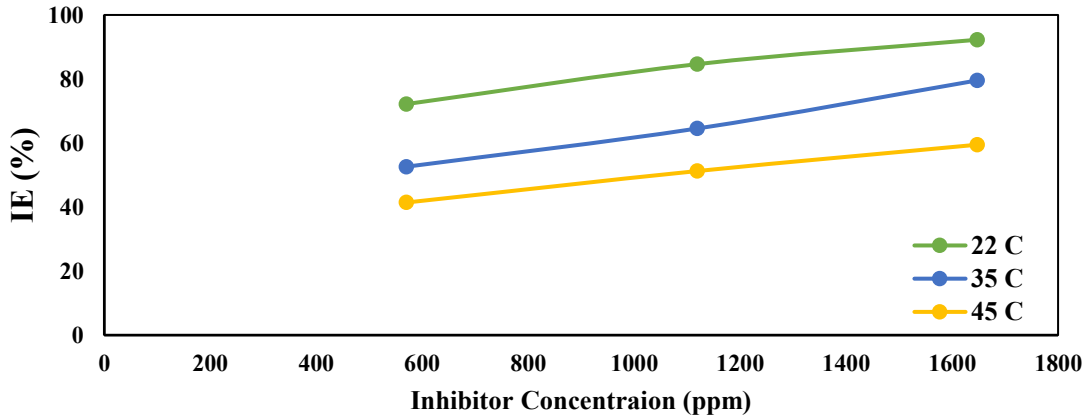

Fig. 5. The effect of temperature on inhibitive efficiency of sage extract for mild steel corrosion in 1 M Sulfuric Acid.

Figure 6 shows the corresponding Arrhenius plots. The activation energy (E_a) calculated from the slope of these plots was 60.29 kJ/mol^{-1} in the absence of sage extract and 94.21 kJ/mol^{-1} in its presence (**Table 6**). The increasing in E_a upon addition of sage extract indicates that the inhibitor interacts with the metal surface through a physical adsorption mechanism.It should be noted that this gives an apparent reaction order and it does not signify which reaction order has occurred. The corrosion rate was determined by calculating from the average weight loss data taken over the time of immersion. Due to a relatively constant corrosion rate within the temperature range investigated (22–45 °C) and no noticeable changes in the corrosion mechanism, it is reasonable to apply the Arrhenius equation.

Figure 7 shows plots of ln(CR/T) vs 1/T for mild steel immersed in an acidic corrosive solution, both with and without the addition of 1647 ppm of sage extract; these plots were produced using the transition-state equation presented in Section 2. As evidenced by the linearity of the plots shown in **Figure 7**, it can be concluded that within the examined temperature range (22-45°C), the corrosion of mild steel has followed the transition-state model; therefore, a single major corrosion mechanism was operational within this temperature range. Further analysis of the slope and intercept of each linearized plot permitted the calculation of the activation enthalpy (ΔH) and activation entropy (ΔS) values as shown in **Table 6**. The negative ΔH values obtained for the sage extract treated mild steel demonstrate that the corrosion process under investigation is exothermic in nature (Sattari et al., 2025). The data obtained also illustrates that as the temperature increases, the adsorption of the constituents of the extract onto the mild steel surface become less favored, suggesting that the primary mode of adsorption of the extract onto the mild steel surface is physical adsorption (Adamu et al., 2025). Additionally, the observed negative ΔS values indicate a reduction in the degree of disorder associated with the formation of the activated complex relative to the reactants (Sattari et al., 2025). The above behavior is indicative of an associative corrosion mechanism in which the activated complexes form via an ordered arrangement of species at the metal/solution interface. Furthermore, the reduction in entropy indicates that the transition state represents a more highly organized configuration than the reactants, likely resulting from the adsorption of inhibitor molecules onto the active corrosion sites. Finally, the differences between the blank and inhibited systems clearly illustrate how the corrosion kinetics have been influenced by the presence of the sage extract. The addition of the extract has modified the activation parameters indicating that the inhibitor has altered the energy barrier of the corrosion reaction and supports the formation of a protective adsorbed layer on the mild steel surface.

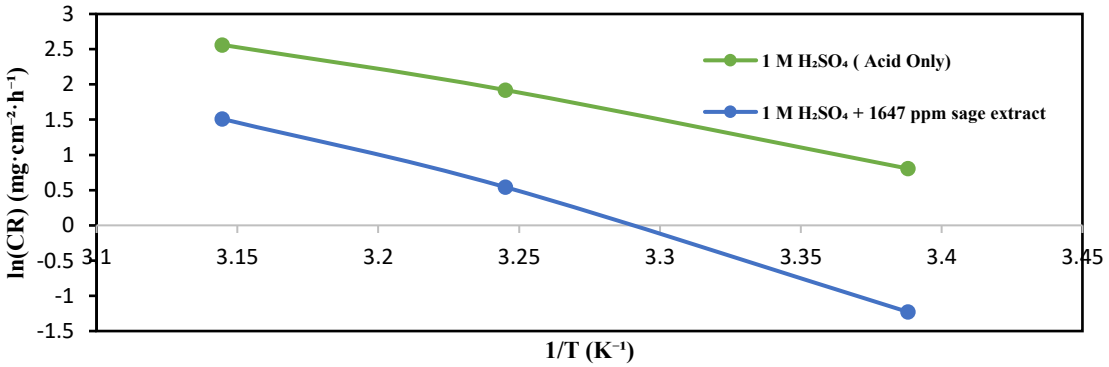

Fig. 6. Arrhenius plot of mild steel corrosion in 1 M sulfuric acid, wilt different temperatures at 1647 ppm of Sage extract in 1M sulfuric acid.

Table 6. Activation parameters (E_a, ΔH, and ΔS) for mild steel in the corrosive acid medium of sage extract

Experimental condition	Concentration (ppm)	E_a, KJ/mol	-ΔH, kJ/mol	-ΔS, kJ/mol
Acid Only	1 M, H_2SO_4	60.29	57. 57	42.28
Acid + Extract	1 M H_2SO_4 + 1647 ppm, sage extract	94.21	91.68	55.9

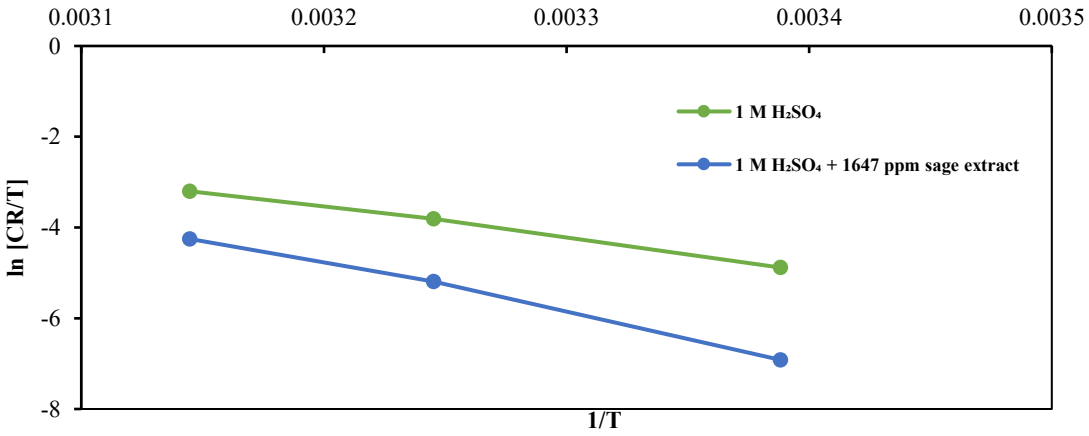

Fig. 7. Plotting of ln [CR/T] against 1/T for mild steel in the acid corrosive medium without and with 1647 ppm of Sage extract.

3.4 Adsorption Isotherm

To understand the nature of the interaction between sage extract molecules and the metal surface, different adsorption equation models were applied to the experimental data. These included the Langmuir (Langmuir, 1918), Freundlich (Freundlich, 1906) and Florry-Huggins (Murthy & Vijayaragavan, 2014). **Figure 8** shows the correlation of these models. It is important to note that the adsorption evaluation presented above is indirect. Instead of measuring independently the surface coverage (θ), as it is typically done in an adsorption study, the surface coverage (θ) used in fitting the Langmuir, Freundlich, and Flory-Huggins isotherms was estimated from the weight loss inhibition efficiency, using the equation θ = IE / 100. Therefore, the assumption made with this method is that the decrease in corrosion rate is directly proportional to the fraction of the metal surface that is coated with inhibitor molecules. Thus, the high degree of correlation of the Langmuir isotherm (i.e., R^2 values equal to 0.9999, 0.9963, and 0.9963 at 22 °C, 35 °C, and 45 °C, respectively) clearly shows that under the experimental conditions examined, the inhibitor creates a monolayer on the metal surface, which is consistent with the Langmuir model (Babiker, 2024) (**Figure 8A**).

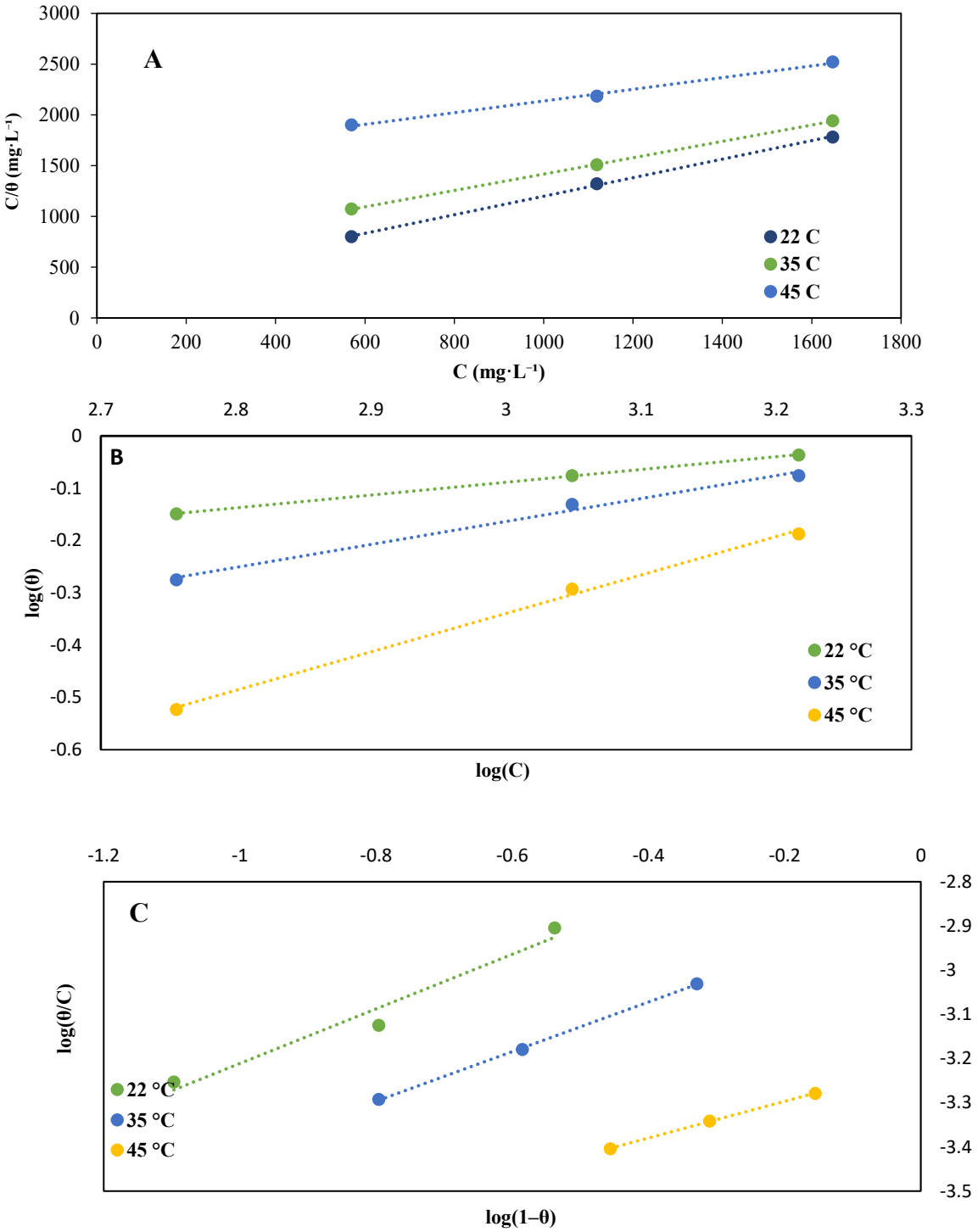

Fig. 8. (A) Langmuir, (B) Freundlich and (C) Florry-Huggins isotherms for the adsorption of sage on the surface of mild steel in 1 M Sulfuric Acid.

Table 7 presents the Langmuir adsorption equilibrium constants, K_{ads} decreased as the temperature increased, from 944.19 L/mol at 22 °C to 172.95 L/mol at 45 °C, indicating low adsorption at double temperatures. This pattern was stabilized with the usual free energy values of adsorption (ΔG°_{ads}), all of which were very poor, confirming the spontaneity of the adsorption process (Babiker, 2024). At 22°C, $\Delta G^{\circ}_{ads}$was -26.66 kJ/mol, compared to -25.89 kJ/mol at 35°C and -24.25 kJ/mol at 45°C. According to thermodynamic criteria, values of ΔG°_{ads} between -20 and 0 kJ/mol usually indicate physical adsorption, while values greater than -40 kJ/mol indicate chemical absorption (Siami et al., 2023). Therefore, the results here point to a spontaneous physical adsorption mechanism.

The Freundlich isotherm, showed in **Figure 8B**, assumes heterogeneous surface adsorption and variable adsorption energies, proved a slight decrease correlation (R^2 = 0.9998, 0.9906 and 0.9968). The Freundlich (n) decreased with temperature (from 4.08 at 22 °C to 1.36 at 45 °C), indicating a decrease in adsorption intensity and surface variation as thermal energy expanded. This also reinforces the conclusion that the damper absorbs more strongly at low temperatures (Xu et al., 2021).

Similarly, the Flory–Huggins's isotherm (**Figure 8C**) was applied to study the size of adsorbed species relative to surface sites. R^2 values were ideal at three applied temperatures (R^2 = 0.9925, 9995 and 9997, respectively). As shown in **Table 7**, the fluorescent-Hoggins adsorption equilibrium constants (K_{fh}) and derived values of ΔG°_{fh} also showed spontaneous adsorption, with values of ΔG°_{fh} -25.88 kJ/mol (22 °C), -25.53 kJ/mol (35 °C), and -24.13 kJ/mol (45 °C). These values also fall within the average range of physical adsorption (Murthy & Vijayaragavan, 2014).

In general, thermodynamic and heat stability data indicate that the green damper is automatically absorbed onto the steel surface, often via a physical adsorption mechanism, forming a protective layer that reduces corrosion. The Langmuir heat stability model describes adsorption behavior well, suggesting single-layer coverage without lateral interaction between molecules. The decrease in the adsorption potential and its constants with increasing temperature shows that the adsorption mechanism is exothermic in nature (Babiker, 2024).

Table 7. Adsorption isotherm parameters

		Temperatures		
Models	**Parameters**	**22°C**	**35°C**	**45°C**
Langmuir	K_{ads} (L/mol)	944.19	441.76	172.95
	ΔG°_{ads} (kJ/mol)	-26.66	-25.98	-24.25
	R^2	0.9999	0.9993	0.9963
Freundlich	N	4.08	2.27	1.36
	$K_f(L/mg)$	0.15	0.033	0.002
	R^2	0.9998	0.9906	0.9968
Florry-Huggins	K_{fh}(L/mol)	687.81	383.21	162.01
	ΔG°_{fh} (kJ/mol)	-25.88	-25.53	-24.13
	R^2	0.9625	0.9995	0.9997

The van't hoff plot as shown in **Figure 9** was created to find the thermodynamic parameters of the adsorption process. Thermodynamic parameters are the slope and y-intercept from a linear regression of lnKa vs. 1/T; and they can be used to calculate the standard heat of adsorption (ΔH°) and standard entropy of adsorption (ΔS°). ΔH° = -66.9kJ/mol and ΔS°= -270.8 J/mole*K. The negative value for the ΔH° indicates that the adsorption of the inhibitor to mild steel is an exothermic reaction. The negative ΔS° indicate a loss in randomness at the solid-solution interface. Therefore, the data support that adsorption occurs due to the formation of an organized inhibitor layer

on the surface of the metal due to high intermolecular attraction between the inhibitor molecule and the metal surface. This data also provides evidence as to the spontaneous nature of the adsorption and supports the inhibitor's efficacy under the experimental conditions.

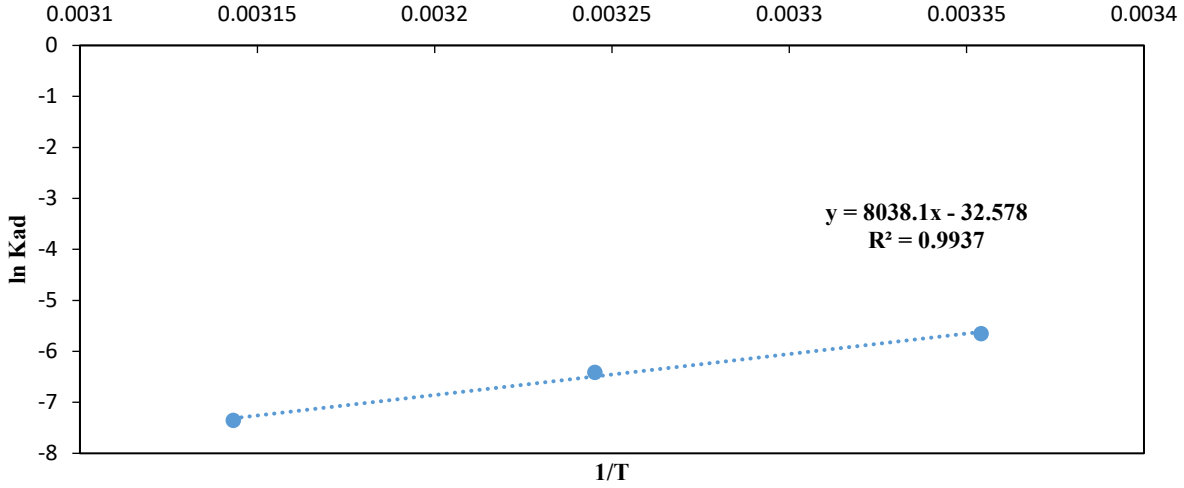

Fig. 9. ln ***k***ad versus temperature (1/T) curve of adsorption inhibiter of mild steel.

The results of this study supported that sage is a good green corrosion inhibitor and its ability to act as one has been shown to be better than it was shown in prior studies where the same extract was used. Compared to other studies (**Table 8**), the present study also found a lower ΔG°ads (−26.66 kJ/mol) for mild steel exposed to 1.0 M H_2SO_4 at 22°C than did Rodriguez-Torres et al., 2015 (−20 kJ/mol), who studied carbon steel in 0.5 M H_2SO_4, and Babiker (−13.73 kJ/mol), who studied zinc in 0.5 M H_2SO_4. A lower ΔG°ads is indicative of greater surface interactions and a more protective film even in more acidic environments.

While the present study also presents improved thermodynamics for adsorption of Sage on mild steel, the present study provides additional information regarding mechanisms of adsorption than prior studies. The application of three different isotherms (Langmuir, Freundlich, and Flory-Huggins) allowed a more complete understanding of adsorption mechanisms including the effects of heterogeneity of surfaces and the possibility of multilayer adsorption. The more detailed analytical treatment presented in the present study will contribute to the scientific community's understanding of sage as an effective, non-toxic, and sustainable corrosion inhibitor.

Table 8. Comparison of Inhibition Efficiency of Various Green Inhibitors in Acidic Media

Green Inhibitor	Acidic Medium	Type of metal	Temperature	ΔG°_{ads}	Reference
Salvia officinalis	1.0 M H_2SO_4	Mild Steel	22	-26.66	Present study
Salvia officinalis	0.5 M H_2SO_4	Carbon Steel	25	-20	(Rodríguez-Torres et al., 2015)
Salvia officinalis	0.5 M H_2SO_4	Zinc	25	-13.73	(Babiker, 2024)

4. Conclusions

This study aimed to evaluate the effectiveness of a green inhibitor in reducing corrosion rates through adsorption on metal surfaces, while exploring the effect of temperature on adsorption behavior. The experimental data were interpreted using three isothermal models of adsorption – Langmuir, Freundlich, and Florry-Huggins to determine the most appropriate model to describe the adsorption mechanism. The Langmuir model tested the highest correlation with the data, indicating single-layer adsorption on a homogeneous surface, while the Freundlich and Florry-Huggins models indicated surface variability and the possibility of forming multiple layers. Thermodynamic analysis showed that all values of the free general adsorption force (ΔG°) were weak, confirming the spontaneous nature of the process and aiding natural adsorption. The results recommend that the green dampers form a strong protective layer on

the steel surface, making it a promising, environmentally friendly and cost-effective alternative to mitigate corrosion in commercial programs.

CRediT Author Contribution Statement

Shatha N. Badarneh: Conceptualization, Writing – Review & Editing, Resources, Visualization, Supervision, Project Administration.
Salah H. Aljbour: Supervision, Project Administration.
Mohammad A. Al-Awamleh: Methodology, Investigation, Writing – Original Draft, Visualization.
Toga T. Al-Btoush: Methodology, Investigation, Writing – Original Draft, Visualization.

Declaration Statements

Funding
This research received no external funding.

Conflicts of Interest
The authors declare no conflict of interest.

Acknowledgement

The corresponding author thanks Prof. Dr. Salah Aljbour for providing the logistic support for the research project.

Nomenclature

Abbreviation	Full Term
AOAC	Association of Official Analytical Chemists
ATR	Attenuated Total Reflectance
FTIR	Fourier Transform Infrared Spectroscopy
HPLC	high-performance liquid chromatograph
UV	Ultraviolet
XRF	X-Ray Florescence

References

Al-Btoush, T. T., Aljbour S. H., Al-AwamlehM. A., & Badarneh S. N. (2026). Investigation of Salvia officialis as a natural corrosion inhibitor for mild steel in sulfuric acid. *Research Journal of Chemistry and Environment.* (Accepted to be published)

Adamu, A. A., Iyun, O. R. A., & Habila, J. D. (2025). Adsorption and thermodynamic studies of the corrosion Inhibition effect of Desmodium adscendens (Swartz) extract on carbon steel in 2 M HCl. *BMC chemistry, 19*(1), 163. https://doi.org/10.1186/s13065-025-01541-y

Ahmed, M. A., Amin, S., & Mohamed, A. A. (2024). Current and emerging trends of inorganic, organic and eco-friendly corrosion inhibitors. *RSC advances, 14*(43), 31877-31920. https://doi.org/10.1039/d4ra05662k

Almahdy, M. S., Molouk, A. F., El-Hossiany, A., & Fouda, A. E.-A. S. (2023). Electrochemical studies of erica arborea extract as a green corrosion inhibitor for C-steel in sulfuric acid medium. *Biointerface Res Appl Chem, 13*(5), 472.https://doi.org/10.33263/BRIAC135.472

Babiker, M. E. (2024). Experimental and computational study of Salvia officinalis leaf extract as an eco-friendly green corrosion inhibitor for zinc in 0.5 M sulfuric acid solution. *Int. J. Corros. Scale Inhib, 13*(3), 1777-1796. https://doi.org/10.17675/2305-6894-2024-13-3-25

Bajrami, D. A., Ganiji, A., Saiti-Musliji, Z., & Jordanovska, S. (2023). A phytochemical analysis of mint and Salvia officinalis L. tea using FTIR technique. *European Journal of Agriculture and Food Sciences, 5*(4), 55-59.https://doi.org/10.24018/ejfood.2023.5.4.682

Christaki, S., Kelesidou, R., Pargana, V., Tzimopoulou, E., Hatzikamari, M., & Mourtzinos, I. (2023). Inclusion complexes of β-Cyclodextrin with Salvia officinalis bioactive compounds and their antibacterial activities. *Plants, 12*(13), 2518.https://doi.org/10.3390/plants12132518

de Souza Morais, W. R., da Silva, J. S., Queiroz, N. M. P., de Paiva e Silva Zanta, C. L., Ribeiro, A. S., & Tonholo, J. (2023). Green corrosion inhibitors based on plant extracts for metals and alloys in corrosive environment: a technological and scientific prospection. *Applied Sciences, 13*(13), 7482.https://doi.org/10.3390/app13137482

Deyab, M., Abdeen, M. M., Hussien, M., E. El-Sayed, I., Galhoum, A., El-Shamy, O. A., & Abd Elfattah, M. (2023). Novel corrosion inhibitor for carbon steel in acidic solutions based on α-Aminophosphonate (Chemical, Electrochemical, and Quantum Studies). *Molecules, 28*(13), 4962.https://doi.org/10.3390/molecules28134962

Eddy, N. O., Ibok, U. J., Garg, R., Garg, R., Iqbal, A., Amin, M., Mustafa, F., Egilmez, M., & Galal, A. M. (2022). A brief review on fruit and vegetable extracts as corrosion inhibitors in acidic environments. *Molecules, 27*(9), 2991.https://doi.org/10.3390/molecules27092991

El Euch, S. K., Hassine, D., Cazaux, S., Bouzouita, N., & Bouajila, J. (2019). Salvia officinalis essential oil: Chemical analysis and evaluation of anti-enzymatic and antioxidant bioactivities. *South African Journal of Botany, 120*, 253-260.https://doi.org/10.1016/j.sajb.2018.07.010

Freundlich, H. M. F. (1906). Over the adsorption in solution. *J. Phys. chem, 57*(385471), 1100-1107.

Girish, C. R. (2025). Determination of thermodynamic parameters in adsorption studies: a review. *Chemical Papers*, 1-20.https://doi.org/10.1007/s11696-025-04218-x

Ibrahim, S., Sanmugapriya, R., Selvi, J. A., Malini, T. P., Kamaraj, P., Vivekanand, P., Periyasami, G., Aldalbahi, A., Perumal, K., & Madhavan, J. (2022). Effect of 3-Nitroacetophenone on Corrosion Inhibition of Mild Steel in Acidic Medium. *International Journal of Photoenergy, 2022*(1), 7276670. https://doi.org/10.1155/2022/7276670

Ituen, E., Akaranta, O., & James, A. (2017). Evaluation of performance of corrosion inhibitors using adsorption isotherm models: an overview. *Chem. Sci. Int. J, 18*(1), 1-34. https://doi.org/10.9734/CSIJ/2017/28976

Javidi, M., Abadeh, H. K., Namazi, F., Yazdanpanah, H. R., & Shiri, N. S. (2024). A new perspective on the corrosion of carbon steels in H2SO4 acid environments: Statistical analysis of corrosion mechanisms by response surface modeling. *Materials Chemistry and Physics, 312*, 128608.https://doi.org/10.1016/j.matchemphys.2023.128608

Langmuir, I. (1918). The adsorption of gases on plane surfaces of glass, mica and platinum. *Journal of the American Chemical society, 40*(9), 1361-1403.https://doi.org/10.1021/ja02242a00

Lavanya, M., Suvarna, A. S., & Kumari, P. P. (2024). Adsorption and corrosion inhibition behaviour of Pterocarpus marsupium stem extract on mild steel in acid medium: experimental and statistical approach. *Canadian Metallurgical Quarterly, 63*(4), 1335-1346. https://doi.org/10.1080/00084433.2023.2273705

Mamedov, I., Shikhaliyeva, I., Mamedova, Y., Gasimova Sh, Z., & Maharramov, A. (2019). Some acetophenone derivatives as corrosion inhibitors. *Kimya Problemleri*(2), 302-309.https://doi.org/10.32737/2221-8688-2019-2-302-309

McCleary, B. V. (2023). Measurement of dietary fiber: Which AOAC Official Method of Analysis SM to use. *Journal of AOAC International, 106*(4), 917-930.https://doi.org/10.1093/jaoacint/qsad051

Mo, S., Luo, H.-Q., & Li, N.-B. (2016). Plant extracts as "green" corrosion inhibitors for steel in sulphuric acid. *Chemical Papers, 70*(9), 1131-1143.https://doi.org/10.1515/chempap-2016-0061

Murthy, Z., & Vijayaragavan, K. (2014). Mild steel corrosion inhibition by acid extract of leaves of Hibiscus sabdariffa as a green corrosion inhibitor and sorption behavior. *Green Chemistry Letters and Reviews, 7*(3), 209-219.https://doi.org/10.1080/17518253.2014.924592

Nikitas, P. (1984). Generalized Flory–Huggins isotherms for adsorption from solution. *Journal of the Chemical Society, Faraday Transactions 1: Physical Chemistry in Condensed Phases, 80*(12), 3315-3329.https://doi.org/10.1039/F19848003315

Ou, G., Cao, X., Mohammed, Y. M., & Wu, W. (2025). Failure Analysis and Corrosion Resistance of Carbon Steel Pipelines in Concentrated Sulfuric Acid. *Metals, 15*(5), 506. https://doi.org/10.3390/met15050506

Panossian, Z., de Almeida, N. L., de Sousa, R. M. F., de Souza Pimenta, G., & Marques, L. B. S. (2012). Corrosion of carbon steel pipes and tanks by concentrated sulfuric acid: a review. *Corrosion Science, 58*, 1-11.https://doi.org/10.1016/j.corsci.2012.01.025

Parangusan, H., Bhadra, J., & Al-Thani, N. (2021). A review of passivity breakdown on metal surfaces: influence of chloride-and sulfide-ion concentrations, temperature, and pH. *Emergent Materials, 4*(5), 1187-1203.https://doi.org/10.1007/s42247-021-00194-6

Rodríguez-Torres, A., Valladares-Cisneros, M., & Gonzalez-Rodríguez, J. (2015). Use of Salvia officinalis as green corrosion inhibitor for carbon steel in acidic media. *International Journal of Electrochemical Science, 10*(5), 4053-4067.https://doi.org/10.1016/S1452-3981(23)06601-4

Sattari, R., Khayati, G. R., & Darezereshki, E. (2025). Electrochemical-surface and theoretical investigations of the interactions of Salvia officinalis extract as a green and sustainable corrosion inhibitor and zinc cations for corrosion protection of carbon steel in sodium chloride solution. *Journal of Molecular Liquids, 433*, 127962.https://doi.org/10.1016/j.molliq.2025.127962

Sellami, I. H., Rebey, I. B., Sriti, J., Rahali, F. Z., Limam, F., & Marzouk, B. (2012). Drying sage (Salvia officinalis L.) plants and its effects on content, chemical composition, and radical scavenging activity of the essential oil. *Food and Bioprocess Technology, 5*(8), 2978-2989.https://doi.org/10.1007/s11947-011-0661-0

Siami, H., Razmkhah, M., & Moosavi, F. (2023). Cation functional group effect on SO2 absorption in amino acid ionic liquids. *Frontiers in Chemistry, 11*, 1113394. https://doi.org/10.3389/fchem.2023.1113394

Singh, P., Srivastava, V., & Quraishi, M. (2016). Novel quinoline derivatives as green corrosion inhibitors for mild steel in acidic medium: electrochemical, SEM, AFM, and XPS studies. *Journal of Molecular Liquids, 216*, 164-173.https://doi.org/10.1016/j.molliq.2015.12.086

Talha, M. (2025). Biomacromolecules as green corrosion inhibitors: a review based on mild steel corrosion in acidic media. *Corrosion Reviews, 43*(4), 409-428.https://doi.org/10.1515/corrrev-2024-0067

Wang, B., Qiu, F., Chen, L., Zhou, Q., Dong, B., Yang, H., Yang, J., Feng, Z., Tyrer, N., & Barber, G. C. (2022). Microstructure and shearing strength of stainless steel/low carbon steel joints produced by resistance spot welding. *Journal of Materials Research and Technology, 20*, 2668-2679.https://doi.org/10.1016/j.jmrt.2022.08.041

Xu, Y., Xu, Z., Guo, Y., Huang, X., Dong, Y., & Li, Q. (2021). Dynamic properties and energy dissipation study of sandwich viscoelastic damper considering temperature influence. *Buildings, 11*(10), 470.https://doi.org/10.3390/buildings11100470